# An Integral Equation-Based Approach to Analyzing Symmetrical Electromagnetic Models Through Decomposition and Recomposition of Excitation Vectors

**Jianxun Su [1], Zhengrui Li [1], Yaoqing (Lamar) Yang [2], and Guizhen Lu [1]**

[1] Department of Information Engineering
Communication University of China, Beijing, 100024, China
sujianxun_jlgx@163.com, lizengrui@cuc.edu.cn, luguizhen@cuc.edu.cn

[2] Department of Computer and Electronics Engineering
University of Nebraska-Lincoln, NE, 68182, USA
yyang3@unl.edu

***Abstract*** ─ In this paper, an Integral Equation-based Simplification Method (IE-SM) is presented for the efficient analysis of the symmetrical electromagnetic model. The proposed approach stems from the decomposition and recomposition of any arbitrary excitation sources into a set of independent vectors which induce a symmetrical current distribution. Compared to the Conventional Integral Equation (CIE) method for modeling an entire structure, this simplification method not only saves computation resources and time by reducing the number of unknowns, but also maintains the computation accuracy. In addition, this method has a simple integral equation formulation, so it can be easily accelerated with fast algorithms and integrated into the existing Method of Moments (MoM) codes. Numerical examples show that the proposed method demonstrates both satisfactory accuracy and efficiency with less computational complexity.

***Index Terms*** ─ Integral equation, recomposition, symmetry model, vector decomposition.

## I. INTRODUCTION

Method of Moments (MoM)-based integral equation solvers are widely used for analyzing time-harmonic electromagnetic radiation and scattering problems. For a practical electromagnetic problem, many targets, such as tank, aircraft, missile, and some microwave & optical devices have elegant symmetric property. To take advantage of the symmetry, the numerical model can be simplified and the number of the unknowns can be greatly reduced. In [1], Lobry, et al., proposed a simplification method for rotational symmetry models with the boundary element method. In [2] and [3], Naito, et al., also made a great contribution to the simplification of symmetry model. The impedance matrix can be transformed to a bordered block diagonal matrix by using spatial eigenmodes transformation. A similar approach with discrete Fourier transform matrix has been reported [4]. However, for an electrically large problem, the matrix transformation process requires huge physical memory and longer computation time. Matrix transformation is difficult to be accelerated by fast multipole algorithms or other related algorithms. Therefore, it is not suitable for an electrically large problem. Furthermore, this transformation is too complicated to be integrated into the existing MoM code [5].

Commercial electromagnetic software such as Ansoft HFSS/Designer, Agilent ADS, EMSS FEKO, CST etc., uses electric and magnetic symmetry planes to simplify the symmetrical electromagnetic model [6]-[8]. The prerequisite of the application of magnetic or electric symmetry planes is the symmetrical distribution of the induced fields, which requires both geometry and excitation sources to be identically symmetrical. Therefore, when using magnetic or electric

*Submitted On: November 26, 2013*
*Accepted On: October 5, 2014*

symmetry planes, geometry and excitations should be symmetrical. The requirement of symmetry excitations severely limits the use of magnetic and electric symmetrical planes of commercial electromagnetic software.

In this paper, an effective simplification method for the symmetrical electromagnetic model is presented. The excitation vector is decomposed and recomposed into a set of independent vectors. For each new excitation vector, the induced current distribution is symmetrical, so that only a part of the induced current needs to be computed. This approach employs a simple integral equation in which one field triangle corresponds to multiple source triangles. Therefore, it is easy to interface with fast algorithms and integrate with the existing MoM codes. Moreover, the current continuity at the truncated boundary of the simplified model is described in detail. A new basis function is derived from the Rao-Wilton-Glisson (RWG) basis function, which is more suitable to achieve the current continuity at the truncated boundary.

## II. PROBLEM FORMULATION

### A. Integral-equation and basis function

Let $S$ be the surface of a metallic object. By enforcing the boundary conditions on the Perfect Electric Conductor (PEC) surface $S$, the Mixed-Potential Integral Equation (MPIE) is given as [9]:

$$-\hat{n}\times\vec{E}^{inc}=\hat{n}\times\left[-j\omega\ddot{G}_A\otimes\vec{J}+\frac{1}{j\omega}(\nabla G_V)\otimes(\nabla'\vec{J})\right], \quad (1)$$

where $\vec{E}^{inc}$ is the incident electric field, $\hat{n}$ is the outside unit normal to $S$, $\vec{J}$ is the unknown current density on $S$, and $\ddot{G}_A$ and $G_V$ are the vector and scalar potential Green's functions.

Testing equation (1) with basis function can be rewritten in a matrix form as follows;

$$[Z][I]=[V], \quad (2)$$

where [Z] is the impedance matrix. [V] is a voltage excitation vector. [I] is the unique solution to the impedance equation. Specifically, for a plane symmetry structure, impedance matrix [Z] is a multilevel block circulant matrix, where each level is a 2x2 block circulant [10].

There are two kinds of basis functions shown in Fig. 1 [11], the Rao-Wilton-Glisson (RWG) basis function and the half-RWG basis function. The half-RWG basis function is derived from the RWG:

$$f_n(\vec{r})=\begin{cases}(l_n/2A_n^+)\rho_n^+(\vec{r}), & \vec{r}\ inside\ T_n^+\\ (l_n/2A_n^-)\rho_n^-(\vec{r}), & \vec{r}\ inside\ T_n^-\\ 0, & otherwise\end{cases}, \quad (3)$$

where $l_n$ is the length of the common edge, and $A_n^{\pm}$ is the area of triangle $T_n^{\pm}$. Vector $\rho_n^-$ connects the observation point $\vec{r}$ to the free vertex of the minus triangle. Vector $\rho_n^+$ connects the free vertex of plus triangle to the observation point. The red line in Fig. 1 stands for the common edge of two adjacent triangles. Half-RWG consists only of one triangle facet.

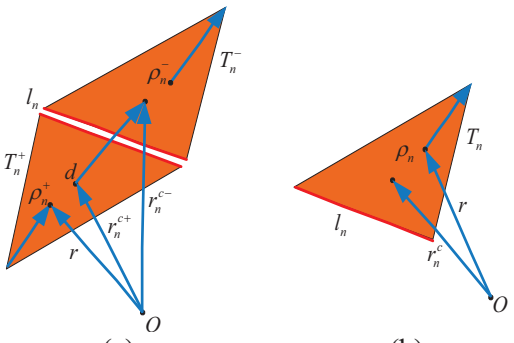


Fig. 1. Two kinds of basis function: (a) RWG basis function, and (b) half-RWG basis function.

### B. Decomposition of plane wave excitation vector

In this paper, a plane wave is taken as the excitation source to introduce the presented method. Considering a scattering problem, the voltage vector is given by [12, eq. (2.8)]:

$$V_m=l_m\left(\vec{E}_m^+\vec{\rho}_m^{c+}/2+\vec{E}_m^-\vec{\rho}_m^{c-}/2\right),$$
$$\vec{E}_m^{\pm}=E^{inc}\left(\vec{r}_m^{c\pm}\right),\quad m=1,\ldots,N, \quad (4)$$

where

$$\vec{\rho}^c=\hat{x}\rho_x^c+\hat{y}\rho_y^c+\hat{z}\rho_z^c$$
$$\vec{r}^c=\hat{x}r_x^c+\hat{y}r_y^c+\hat{z}r_z^c$$

$\vec{E}^{inc}$ is the electric field of an incident electromagnetic signal; the voltage excitation vector is similar to the circuit voltage with units of Vm. The dot product in equation (4) is expanded as follows:

$$\vec{E}\vec{\rho}^c=\left(\vec{\rho}^c\vec{E}_0\right)e^{-j\vec{k}\vec{r}^c}$$
$$=(A+B+C)\left[D+E+F+G-j(H+I+J+K)\right], \quad (5)$$

where

$$A = E_{0x}\rho_x^c,\ B = E_{0y}\rho_y^c,\ C = E_{0z}\rho_z^c,$$
$$D = \cos(k_x r_x^c)\cos(k_y r_y^c)\cos(k_z r_z^c),$$
$$E = -\sin(k_x r_x^c)\sin(k_y r_y^c)\cos(k_z r_z^c),$$
$$F = -\sin(k_x r_x^c)\cos(k_y r_y^c)\sin(k_z r_z^c),$$
$$G = -\cos(k_x r_x^c)\sin(k_y r_y^c)\sin(k_z r_z^c),$$
$$H = -\sin(k_x r_x^c)\cos(k_y r_y^c)\cos(k_z r_z^c),$$
$$I = -\cos(k_x r_x^c)\sin(k_y r_y^c)\cos(k_z r_z^c),$$
$$J = -\cos(k_x r_x^c)\cos(k_y r_y^c)\sin(k_z r_z^c),$$
$$K = \sin(k_x r_x^c)\sin(k_y r_y^c)\sin(k_z r_z^c).$$

According to the linear system characteristics of a plane symmetry structure, the excitation vectors needs to be decomposed and recomposed into a set of new independent vectors. For each new vector, a MoM linear system can obtain an efficient solution.

## III. CLASSIFICATION AND SIMPLIFICATION OF SYMMETRY STRUCTURES

The structure of plane symmetry can be divided into three categories as shown in Fig. 2. The number of symmetry planes of an isosceles triangle, a rectangular, and a sphere, are one, two and three respectively. The symmetry planes are orthogonal to each other.

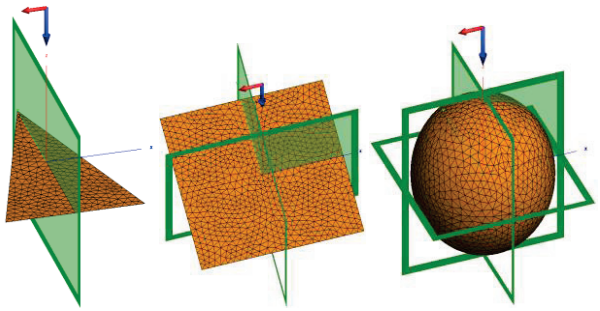

(a) (b) (c)

Fig. 2. Classification of symmetry structures: (a) single symmetry plane, (b) double symmetry planes, and (c) triple symmetry planes.

### A. Single symmetry plane

An isosceles triangle patch is taken as an example of a single symmetry plane. It is symmetrical about the yoz-plane shown in Fig. 3.

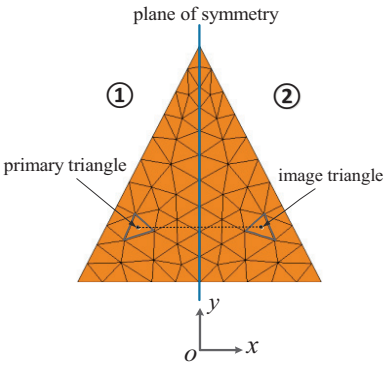


Fig. 3. Isosceles triangle patch.

The model of a single symmetry plane is divided into two subregions. The impedance matrix is a 2x2 block circulant matrix. The simultaneous equations are set up as follows:

$$\begin{bmatrix}\{Z_{11}\} & \{Z_{12}\}\\ \{Z_{12}\} & \{Z_{11}\}\end{bmatrix}\times\begin{bmatrix}\{I_1\}\\ \{I_2\}\end{bmatrix}=\begin{bmatrix}\{V_1\}\\ \{V_2\}\end{bmatrix}, \tag{6}$$

where

$$\{V_1\} = (AD - AE - AF - AG + BD - BE - BF - BG + CD - CE - CF - CG) - j(AH + AI + AJ - AK + BH + BI + BJ - BK + CH + CI + CJ - CK),$$
$$\{V_2\} = (AD + AE - AF + AG - BD - BE + BF - BG + CD + CE - CF + CG) - j(AH - AI + AJ + AK - BH + BI - BJ - BK + CH - CI + CJ + CK).$$

They can also be recomposed as follows:

$$\{V_1\} = \{\kappa_1\} + \{\kappa_2\}, \tag{7}$$
$$\{V_2\} = \{\kappa_1\} - \{\kappa_2\}, \tag{8}$$

where

$$\{\kappa_1\} = (AD - AF - BE - BG + CD - CF) - j(AH + AJ + BI - BK + CH + CJ),$$
$$\{\kappa_2\} = -(AE + AG - BD + BF + CE + CG) - j(AI - AK + BH + BJ + CI - CK).$$

Therefore, excitation vector [V] in equation (2) can be decomposed into two new independent vectors [13] as follows:

$$[V_1] = \begin{bmatrix}\{\kappa_1\}\\ \{\kappa_1\}\end{bmatrix}, \tag{9}$$

$$[V_2]=\begin{bmatrix}+\{\kappa_2\}\\-\{\kappa_2\}\end{bmatrix}. \tag{10}$$

The sign relationship of two new excitation vectors between two subregions of the geometry model is shown in Table 1.

Table 1: Sign relationship of new excitation vectors

| Subregion | $[V_1]$ | $[V_2]$ |
|---|---|---|
| ① | + | + |
| ② | + | − |

(1) Computing the induced current of excitation vector $[V_1]$.

Because the impedance matrix is 2x2 block circulant matrix, the sign of current expansion coefficients is the same as that of the excitation vector. We can obtain the current expansion coefficient relationship between two subregions as illustrated in Fig. 4:

$$\{I_1\}=\{I_2\}. \tag{11}$$

Because two subregions of the electromagnetic model have the same current coefficient, only one half of the current in this model needs to be solved. Consequently, the impedance matrix of the Mixed-Potential Integral Equation (MPIE) is given by:

$$Z_{mn}=\sum_{k=1}^{2}c(k)\Big\{j\omega\langle f_m,\ddot{G}_A\otimes f_{nk}\rangle +\frac{1}{j\omega}\langle\nabla f_m,G_V\otimes(\nabla' f_{nk})\rangle\Big\}, \tag{12}$$

where

$$c(k)=1,\ if\ k=1,2.$$

One field triangle corresponds to two source triangles as shown in Fig. 4. $f_{n1}$ is the basis function of primary source triangle $n_1$; $f_{n2}$ is the basis function of the other source triangle $n_2$, respectively.

The current of two parts have the relationship as follows:

$$\vec{I}_{1x}=-\vec{I}_{2x}, \tag{13}$$

$$\vec{I}_{1y}=\vec{I}_{2y}. \tag{14}$$

As shown in Fig. 4, there is no current flowing through the symmetry plane (yoz-plane). Symmetry plane is equivalent to PEC plane. Therefore, the triangle facets connecting yoz-plane are not assigned for the half-RWG basis function.

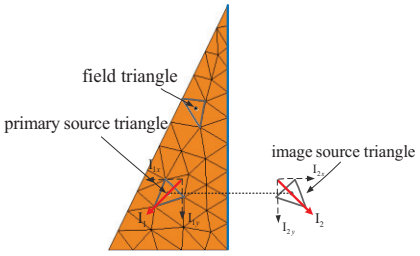


Fig. 4. The field and source triangles. Red arrows are the current direction of the two source triangles.

(2) Computing the induced current of excitation vector $[V_2]$.

We can further derive the current coefficients relationship between two subregions shown in Fig. 5:

$$\{I_1\}=-\{I_2\}. \tag{15}$$

Consequently, only one half of the model needs to be analyzed. The impedance matrix of the Mixed-Potential Integral Equation (MPIE) is given by:

$$Z_{mn}=\sum_{k=1}^{2}\Big\{c(k)\,j\omega\langle f_m,\ddot{G}_A\otimes f_{nk}\rangle +\frac{1}{j\omega}\langle\nabla f_m,G_V\otimes(\nabla' f_{nk})\rangle\Big\}, \tag{16}$$

where

$$c(k)=\begin{cases}1, & if\ k=1\\ -1, & if\ k=2\end{cases}.$$

One field triangle corresponds to two source triangles, as shown in Fig. 5.

There is normal current flowing through the yoz-plane (blue line). The symmetry plane is equivalent to a Perfect Magnetic Conductor (PMC) plane. Therefore, to ensure current continuity at the truncated boundary, the triangle facets connecting the yoz-plane should be assigned by the half-RWG basis function.

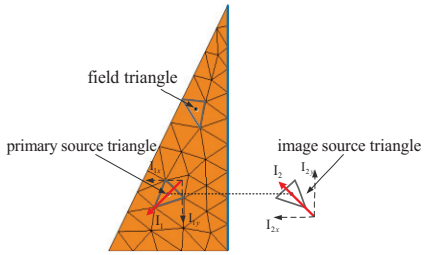


Fig. 5. The field and source triangles. Red arrows are the current direction of the two source triangles.

The assignment of half-RWG basis functions to the triangle facets connected to symmetry plane for different excitation vectors is summarized in Table 2. If there is normal current flowing through the symmetry plane, half-RWG basis functions are assigned to ensure the current continuity at the truncated edges.

Table 2: Assigned case of half-RWGs

| | [V1] | [V2] |
|---|---|---|
| yoz-plane | | H |

(*H denotes half-RWG)

### B. Double symmetry plane

Here, the rectangular patch is taken as an example of double symmetry planes. It is symmetrical about the xoz-plane and yoz-plane, as shown in Fig. 6.

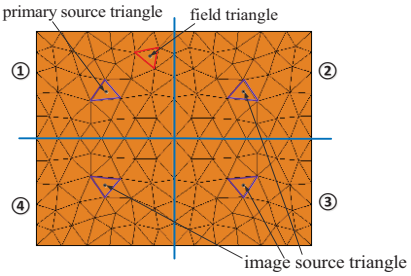


Fig. 6. Rectangular patch.

The model with double symmetry planes is divided into 4 subregions. The impedance matrix is a two-level block circulant matrix where each level is a 2x2 block circulant. The simultaneous equations are set up as follows:

$$\begin{bmatrix} \{Z_{11}\} & \{Z_{12}\} & \{Z_{13}\} & \{Z_{14}\} \\ \{Z_{12}\} & \{Z_{11}\} & \{Z_{14}\} & \{Z_{13}\} \\ \{Z_{13}\} & \{Z_{14}\} & \{Z_{11}\} & \{Z_{12}\} \\ \{Z_{14}\} & \{Z_{13}\} & \{Z_{12}\} & \{Z_{11}\} \end{bmatrix} \times \begin{bmatrix} \{I_1\} \\ \{I_2\} \\ \{I_3\} \\ \{I_4\} \end{bmatrix} = \begin{bmatrix} \{V_1\} \\ \{V_2\} \\ \{V_3\} \\ \{V_4\} \end{bmatrix}. \quad (17)$$

The excitation vector can be recomposed as follows:

$$[V] = \begin{bmatrix} \{V_1\} \\ \{V_2\} \\ \{V_3\} \\ \{V_4\} \end{bmatrix} = \begin{bmatrix} \{\kappa_1\} & +\{\kappa_2\} & +\{\kappa_3\} & +\{\kappa_4\} \\ \{\kappa_1\} & -\{\kappa_2\} & +\{\kappa_3\} & -\{\kappa_4\} \\ \{\kappa_1\} & +\{\kappa_2\} & -\{\kappa_3\} & -\{\kappa_4\} \\ \{\kappa_1\} & -\{\kappa_2\} & -\{\kappa_3\} & +\{\kappa_4\} \end{bmatrix}, \quad (18)$$

where

$$\{\kappa_1\} = (AD - BE - CF) - j(AJ - BE + CH),$$
$$\{\kappa_2\} = (-AE + BD - CG) - j(-AK + BJ + CI),$$
$$\{\kappa_3\} = (-AF - BG + CD) - j(AH + BI + CJ),$$
$$\{\kappa_4\} = (-AG - BF - CE) - j(AI + BH - CK).$$

Therefore, the excitation vector can be decomposed into 4 new independent vectors as follows:

$$[V] = [V_1] + [V_2] + [V_3] + [V_4], \quad (19)$$

where

$$[V_1] = \begin{bmatrix} +\{\kappa_1\} \\ +\{\kappa_1\} \\ +\{\kappa_1\} \\ +\{\kappa_1\} \end{bmatrix}, [V_2] = \begin{bmatrix} +\{\kappa_2\} \\ -\{\kappa_2\} \\ +\{\kappa_2\} \\ -\{\kappa_2\} \end{bmatrix}, [V_3] = \begin{bmatrix} +\{\kappa_3\} \\ +\{\kappa_3\} \\ -\{\kappa_3\} \\ -\{\kappa_3\} \end{bmatrix}, [V_4] = \begin{bmatrix} +\{\kappa_4\} \\ -\{\kappa_4\} \\ -\{\kappa_4\} \\ +\{\kappa_4\} \end{bmatrix}.$$

The sign relationship of new excitation vectors among 4 subregions of the symmetry model is shown in Table 3.

Table 3: Sign relationship of four new excitation vectors

| Subregion | [V1] | [V2] | [V3] | [V4] |
|---|---|---|---|---|
| ① | + | + | + | + |
| ② | + | − | + | − |
| ③ | + | + | − | − |
| ④ | + | − | − | + |

The assignment of half-RWG basis functions to the triangle facets connected to symmetry plane for different excitation vectors is summarized in Table 4. For example, the half-RWG basis should be assigned to the triangle facets connecting to the xoz-plane and the yoz-plane for excitation vector [V2].

Table 4: Assigned case of half-RWGs

| | [V1] | [V2] | [V3] | [V4] |
|---|---|---|---|---|
| xoz-plane | | H | H | |
| yoz-plane | | H | | H |

(*H denotes half-RWG)

### C. Triple symmetry plane

Here, the cuboid is taken as an example of triple symmetry planes. It is symmetrical about the xoy-plane, xoz-plane and yoz-plane, as shown in Fig. 7.

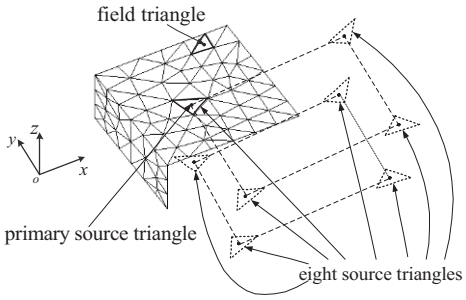


Fig. 7. Metal cuboid.

The model has three symmetry planes, so there are eight symmetrical subregions. The impedance matrix is a three-level block circulant matrix. The simultaneous equations are set up as follows:

$$\begin{bmatrix} \{Z_{11}\} & \{Z_{12}\} & \{Z_{13}\} & \{Z_{14}\} & \{Z_{15}\} & \{Z_{16}\} & \{Z_{17}\} & \{Z_{18}\} \\ \{Z_{12}\} & \{Z_{11}\} & \{Z_{14}\} & \{Z_{13}\} & \{Z_{16}\} & \{Z_{15}\} & \{Z_{18}\} & \{Z_{17}\} \\ \{Z_{13}\} & \{Z_{14}\} & \{Z_{11}\} & \{Z_{12}\} & \{Z_{17}\} & \{Z_{18}\} & \{Z_{15}\} & \{Z_{16}\} \\ \{Z_{14}\} & \{Z_{13}\} & \{Z_{12}\} & \{Z_{11}\} & \{Z_{18}\} & \{Z_{17}\} & \{Z_{16}\} & \{Z_{15}\} \\ \{Z_{15}\} & \{Z_{16}\} & \{Z_{17}\} & \{Z_{18}\} & \{Z_{11}\} & \{Z_{12}\} & \{Z_{13}\} & \{Z_{14}\} \\ \{Z_{16}\} & \{Z_{15}\} & \{Z_{18}\} & \{Z_{17}\} & \{Z_{12}\} & \{Z_{11}\} & \{Z_{14}\} & \{Z_{13}\} \\ \{Z_{17}\} & \{Z_{18}\} & \{Z_{15}\} & \{Z_{16}\} & \{Z_{13}\} & \{Z_{14}\} & \{Z_{11}\} & \{Z_{12}\} \\ \{Z_{18}\} & \{Z_{17}\} & \{Z_{16}\} & \{Z_{15}\} & \{Z_{14}\} & \{Z_{13}\} & \{Z_{12}\} & \{Z_{11}\} \end{bmatrix}. \quad (20)$$

The excitation vector can be recomposed as follows:

$$[V] = \begin{bmatrix} \{V_1\} \\ \{V_2\} \\ \vdots \\ \{V_8\} \end{bmatrix} = \begin{bmatrix} \{\kappa_1\}+\{\kappa_2\}+\{\kappa_3\}+\{\kappa_4\}+\{\kappa_5\}+\{\kappa_6\}+\{\kappa_7\}+\{\kappa_8\} \\ \{\kappa_1\}-\{\kappa_2\}+\{\kappa_3\}-\{\kappa_4\}+\{\kappa_5\}-\{\kappa_6\}+\{\kappa_7\}-\{\kappa_8\} \\ \{\kappa_1\}+\{\kappa_2\}-\{\kappa_3\}-\{\kappa_4\}+\{\kappa_5\}+\{\kappa_6\}-\{\kappa_7\}-\{\kappa_8\} \\ \{\kappa_1\}-\{\kappa_2\}-\{\kappa_3\}+\{\kappa_4\}+\{\kappa_5\}-\{\kappa_6\}-\{\kappa_7\}+\{\kappa_8\} \\ \{\kappa_1\}+\{\kappa_2\}+\{\kappa_3\}+\{\kappa_4\}-\{\kappa_5\}-\{\kappa_6\}-\{\kappa_7\}-\{\kappa_8\} \\ \{\kappa_1\}-\{\kappa_2\}+\{\kappa_3\}-\{\kappa_4\}-\{\kappa_5\}+\{\kappa_6\}-\{\kappa_7\}+\{\kappa_8\} \\ \{\kappa_1\}+\{\kappa_2\}-\{\kappa_3\}-\{\kappa_4\}-\{\kappa_5\}-\{\kappa_6\}+\{\kappa_7\}+\{\kappa_8\} \\ \{\kappa_1\}-\{\kappa_2\}-\{\kappa_3\}+\{\kappa_4\}-\{\kappa_5\}+\{\kappa_6\}+\{\kappa_7\}-\{\kappa_8\} \end{bmatrix}, \quad (21)$$

where

$$\{\kappa_1\} = (AD - BE - CF),\ \{\kappa_2\} = (-AE + BD - CG),$$
$$\{\kappa_3\} = (-AF - BG + CD),\ \{\kappa_4\} = (-AG - BF - CE),$$
$$\{\kappa_5\} = -j(AJ - BE + CH),\ \{\kappa_6\} = -j(-AK + BJ + CI),$$
$$\{\kappa_7\} = -j(AH + BI + CJ),\ \{\kappa_8\} = -j(AI + BH - CK).$$

Therefore the excitation vector in equation (2) is decomposed into eight new independent vectors as follows:

$$[V] = [V_1] + [V_2] + \cdots + [V_8]. \quad (22)$$

The sign relationship of the excitation vector among 8 subregions of the symmetry model is shown in Table 5.

Table 5: Sign relationship of eight new excitation vectors

| Subregion | [V1] | [V2] | [V3] | [V4] | [V5] | [V6] | [V7] | [V8] |
|---|---|---|---|---|---|---|---|---|
| ① | + | + | + | + | + | + | + | + |
| ② | + | - | + | - | + | - | + | - |
| ③ | + | + | - | - | + | + | - | - |
| ④ | + | - | - | + | + | - | - | + |
| ⑤ | + | + | + | + | - | - | - | - |
| ⑥ | + | - | + | - | - | + | - | + |
| ⑦ | + | + | - | - | - | - | + | + |
| ⑧ | + | - | - | + | - | + | + | - |

Table 6 shows the half-RWG basis functions, which are assigned to the triangle facets connected to the truncated edges for different excitation vectors.

Table 6: Assigned case of half-RWGs

| | [V1] | [V2] | [V3] | [V4] | [V5] | [V6] | [V7] | [V8] |
|---|---|---|---|---|---|---|---|---|
| xoy-plane | | | | | H | H | H | H |
| xoz-plane | | H | H | | | H | H | |
| yoz-plane | | H | | H | | H | | H |

(*H denotes half-RWG)

The above analyses on three categories of plane-symmetry structure utilize a plane wave as the excitation. In practical electromagnetic applications, there are many other kinds of excitation sources, such as waveguide excitation, electric/magnetic point source, and aperture field source etc. For those excitation sources, the excitation vector of MoM linear system can also be decomposed and recomposed into a set of independent vectors with the aforementioned relationship. Therefore, the proposed approach can be used to effectively analyze symmetrical

electromagnetic models without the constraints of excitation sources.

## IV. COMPUTATIONAL COMPLEXITY

Assume that the number of symmetrical subregions is *N*, the number of unknowns in each subregion is *M*, and the number of iterations to reach convergence is *k*.

The total unknown of CIE is *NM*. The complexity of matrix filling, storage and iterative solution are $o(N^2M^2)$, $o(N^2M^2)$ and $o(kN^2M^2)$, respectively.

For IE-SM, for the calculation of each impedance matrix element, one field triangle corresponds to *N* source triangles, so that *N* submatrices need to be calculated and stored. Therefore, complexity of matrix filling and storage becomes $o(NM^2)$. Actually, the matrix filling time of IE-SM would be less than $1/N$ of that of CIE. In terms of memory usage, IE-SM is $1/N$ of CIE.

In the Krylov iterative solution process, MoM linear system needs to be solved *N* times because the excitation vector is decomposed into *N* new independent vectors. Thus, complexity of the iterative solution is $o(NkM^2)$. As a result of less unknowns, IE-SM achieves more stable and rapid convergence than CIE. Actually, computation time of IE-SM is much less than $1/N$ of that of the CIE method. The comparison of the computational complexity of IE-SM and CIE is summarized in Table 7.

Table 7: Complexity statistics

| | Memory | Matrix Filling Time | Iterative Solution Time |
|---|---|---|---|
| CIE | $o\left(N^2M^2\right)$ | $o\left(N^2M^2\right)$ | $o\left(kN^2M^2\right)$ |
| IE-SM | $o\left(NM^2\right)$ | $o\left(NM^2\right)$ | $o\left(kNM^2\right)$ |

## V. NUMERICAL SIMULATIONS

To validate the accuracy and the efficiency of the proposed approach, four numerical simulations are presented in this section. These simulations include the electromagnetic wave scatterings from a metallic sphere and a missile model, electromagnetic wave transmission through a cross-shaped quasi-optical filter, and electromagnetic wave radiation from a pyramidal horn antenna. All numerical experiments run on a HP mini workstation with quad-core 64-bit Intel i7-870 CPU and 16 GB of RAM. The resulting impedance matrices are iteratively solved using the GMRES (80) solver [14], where 80 is the restart number and the relative error tolerance is set to be $10^{-3}$.

### A. Metal sphere

For the first simulation, a metal sphere as shown in Fig. 8 was analyzed using the proposed simplification method. In the simulation, only one-8th of the model needs to be calculated. Our simulation results of bistatic Radar Cross-Section (RCS) agree very well with that of Mie series solution shown in Fig. 9. The normalized induced current distributions of the CIE and IE-SM method are compared in Fig. 10, and a good agreement can be observed. The one-8th model was discretized into 476 triangles, and the average side length of the triangle facets was about one-tenth of the wavelength. The matrix filling and solving time are only 3.1 and 6.8 s, respectively. The corresponding CPU time on the same PC is 26.4 and 141.8 s for modeling the whole structure with 3808 triangle facets. The number of iterations required for the norm of the relative residual to fall below $10^{-3}$ with IE-SM and CIE are 2 and 4, respectively.

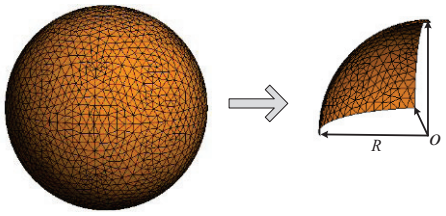


Fig. 8. The model of metal sphere with $R=1\lambda$ is simplified to one-8th model by symmetry.

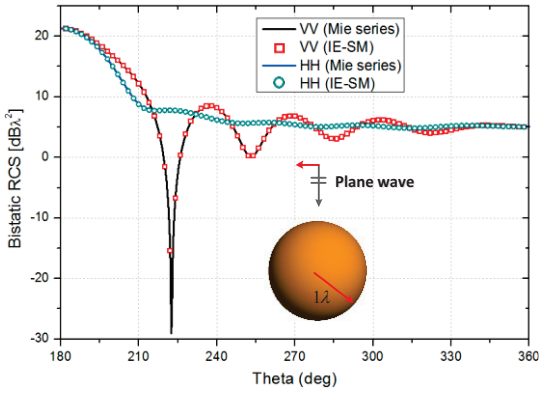


Fig. 9. The bistatic RCS of metal sphere.

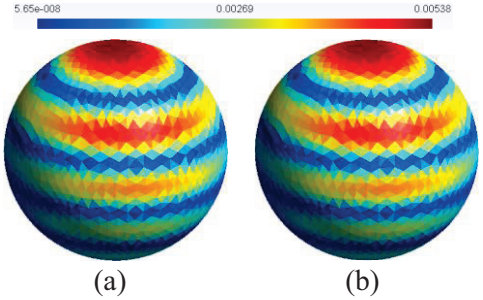


Fig. 10. Normalized current distribution of metal sphere: (a) CIE, and (b) IE-SM.

### B. Missile model

Next, the bistatic RCS of a plane wave incident on a missile model is analyzed. The geometry of the problem is shown in Fig. 11. The bistatic RCS for a plane wave with vertical polarization at oblique incidence ($\theta^{inc}=45^0, \varphi^{inc}=45^0$) is plotted as a function of observation directions in Fig. 12. A very good agreement with the simulated values of modeling the entire structure is validated. Here, the one-4$^{th}$ model was discretized into 2600 triangular cells. The matrix filling and solving time were only 36.6 s and 175.2 s, respectively. The corresponding CPU time was 153.3 s and 2141.8 s for CIE modeling the whole structure. The number of iterations for IE-SM and CIE are 3 and 6, respectively. It is worth mentioning that the magnetic and electric symmetrical planes of commercial electromagnetic software can be used to analyze this missile structure provided the wave propagates along the axis direction of the missile with the E-field parallel to the wing.

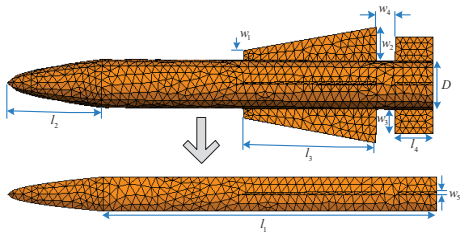


Fig. 11. The missile model is simplified to one-4$^{th}$ model by symmetry. Dimension are in λ: $l_1=7.0$, $l_2=2.0$, $l_3=2.8$, $l_4=0.8$, $w_1=0.2$, $w_2=0.7$, $w_3=0.5$, $w_4=0.4$, $w_5=0.04$, $D=1.0$; the depth of focus of the missile head is 1/32.

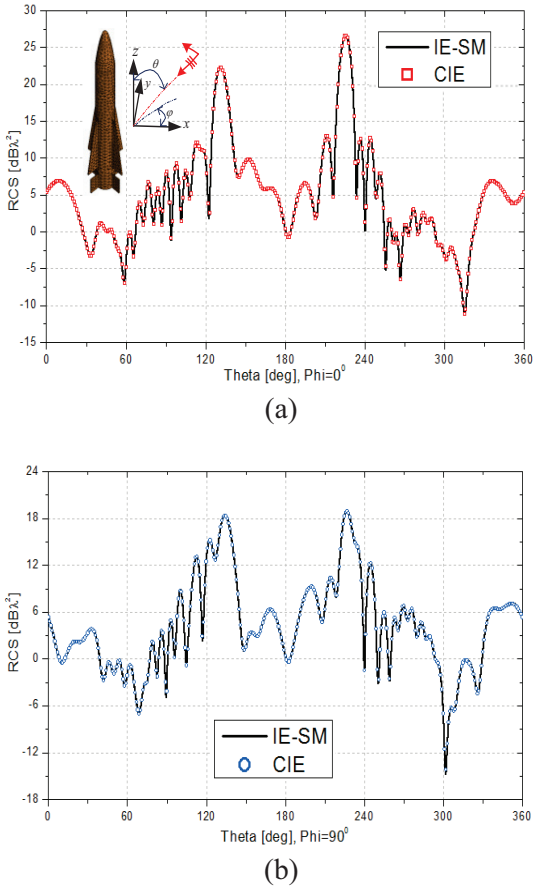


Fig. 12. The bistatic RCS of: (a) xoz-plane, and (b) yoz-plane.

### C. Cross-shaped quasi-optical filter

A bandpass filter comprised of periodic cross-shaped holes with a resonance frequency of 280 GHz was analyzed as follows. The one-4$^{th}$ model shown in Fig. 13 is discretized into 218 triangles to ensure accurate results were obtained throughout the entire frequency band. The transmission coefficients for a plane wave with the E-field parallel to the x-axis at normal incidence (TEMx mode) are plotted as a function of frequency in Fig. 14. Black lines represent the results obtained using our proposed method, red lines represent the results using the simulation from [15], and curves with blue circles represent the measured values. A close agreement between the proposed method and the results in [15] has been achieved. The time for calculating a frequency point is 6.3 s, while it takes up to 28.4 s for computing the whole unit cell.

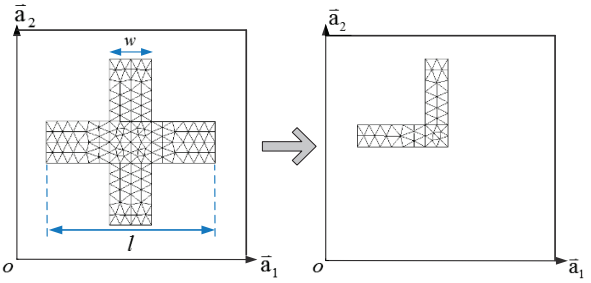


Fig. 13. The unit cell of cross-shaped aperture array is simplified to one-4th model. Dimension are in micrometers (mm): Square lattice period, $\vec{a}_1$=$\vec{a}_2$ = 810, slot length $l$ = 570, slot width $w$=160.

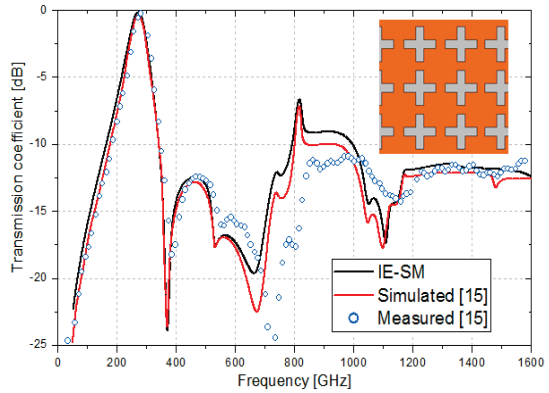


(a)

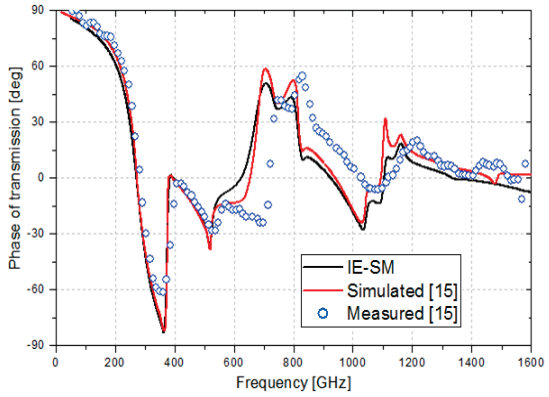


(b)

Fig. 14. (a) Magnitude, and (b) phase of the transmission coefficient.

### D. Horn antenna

Finally, a pyramidal horn antenna [6] operating at the frequency 1.645 GHz was constructed and simulated. An illustration of the horn antenna is shown in Fig. 15. A waveguide mode excitation is applied to the feeding port. The desired mode (in this case a $TE_{10}$ mode) is directly impressed to the rectangular waveguide section denoted by the red line shown in Fig. 15. The mesh size on the back face of the waveguide is one-fifteenth of the wavelength. Figure 16 shows the far field patterns of the E-plane and H-plane computed by IE-SM and the EMSS FEKO [6]. Excellent agreement is observed. Here, the one-4th model was discretized into 1300 triangular cells. The matrix filling and solving time were 9.8 and 77.5 s, respectively. If modeling the whole structure with 5200 triangle facets, the corresponding time of CIE would be 43 and 530 s. The number of iterations for IE-SM and CIE are 5 and 7, respectively.

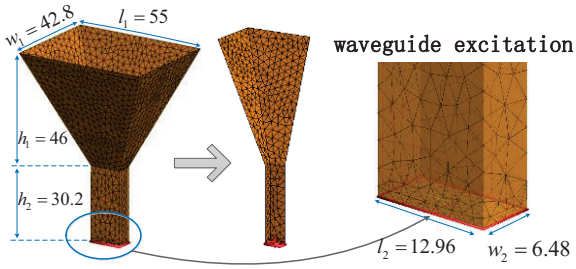


Fig. 15. The model of horn antenna is simplified to one-4th model. Dimension are in centimeters.

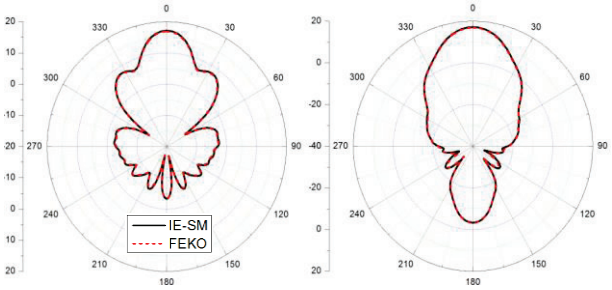


(a) (b)

Fig. 16. The far field pattern: (a) E-plane, and (b) H-plane.

## VI. CONCLUSION

An integral equation-based simplification method is presented for the analysis of electromagnetic targets with plane symmetry. The proposed method does not require excitation resources to be identically symmetrical. It can make the induced current distribution symmetrical by decomposing and recomposing the excitation vector. Consequently, this method greatly reduces

the simulation time and memory usage compared with the Conventional Integral Equation (CIE) method. Numerical experiments validated the accuracy and the computational efficiency of the proposed IE-SM method.

## ACKNOWLEDGMENT

This work was supported in part by the Major Program of the National Natural Science Foundation of China (NSFC) under Grant No. 61331002, in part by the NSFC under Grand No. 61201082, in part by school fund of CUC under Grand No. 3132014XNG1466, and in part by Excellent Innovation Team of CUC under Grand No. yxtd201303.

## REFERENCES

[1] J. Lobry, J. Trecat, and C Broche, "Broken symmetry in the boundary element method," *IEEE Trans. Magn*., vol. 31, no. 3, May 1995.

[2] H. Tsuboi, A. Sakurai, and T. Naito, "A simplification of boundary element model with rotational symmetry in electromagnetic field analysis," *IEEE Trans. Magn*., vol. 26, no. 5, pp. 2771-2773, September 1990.

[3] H. Tsuboi, M. Tanaka, T. Misaki, M. Analoui, T. Naito, and T. Morita, "Reduction of vector unknowns using geometric symmetry in a triangular-patch moment method for electromagnetic scattering and radiation analysis," *IEEE Trans. Magn*., vol. 28, no. 2, March 1992.

[4] G. J. Burke and A. J. Poggio, "Numerical electromagnetics code (NEC)-method of moments," *Lawrence Livermore Laboratory*, January 1981.

[5] T. Naito and H. Tsuboi, "A simplification method for reflective and rotational symmetry model in electromagnetic field analysis," *IEEE Trans. Magn*., vol. 37, no. 5, September 2001.

[6] "User's manual," *FEKO Suite 6.0*, pp. 6-44, September 2010.

[7] *Ansys HFSS12 Full Book*, pp. 3.1-10, January 2010.

[8] *CST MICROWAVE STUDIO*, "*Workflow and solver Overview*," pp. 27-31, 2010.

[9] K. A. Michalski and J. R. Mosig, "Multilayered media Green's functions in integral equation formulations," *IEEE Trans. Antennas Propag*., vol. 45, pp. 508-519, March 1997.

[10] P. J. Davis, "Circulant matrices (2 edition)," *Chelsea Press*, 1994.

[11] S. M. Rao, D. R. Wilton, and A. W. Gilisson, "Electromagnetic scattering by surfaces of arbitrary shape," *IEEE Trans. Antennas Propag*., vol. AP-30, no. 3, pp. 409-518, 1982.

[12] S. N. Makarov, "Antenna and EM modeling with MATLAB," *New York: Wiley*, 2002.

[13] G. Strang, "Introduction to linear algebra," *Wellesley-Cambridge Press*, U.S., 2009.

[14] Y. Saad and M. H. Schultz, "GMRES: a generalized minimal residual algorithm for solving nonsymmetric linear systems," *SIAM J. Sci. Stat. Comput*., vol. 7, no. 3, pp. 856-869, July 1986.

[15] M. Bozzi, L. Perregrini, J. Weinzierl, and C. Winnewisser, "Efficient analysis of quasi-optical filters by a hybrid MoM/BI-RME method," *IEEE Trans. Antennas Propag*., vol. 49, no. 7, pp. 1054-1064, July 2001.

**Jianxun Su** received the M.S. and the Ph.D. degree in Electromagnetic Field and Microwave Technology from the Communication University of China and Beijing Institute of Technology, Beijing, China, in 2008 and 2011, respectively.

From 2011 to 2013, he was with East China Research Institute of Electronic Engineering (ECRIEE), where he engaged in phased-array research. He is currently working as Postdoctoral Fellow at Electromagnetic Laboratory, Communication University of China. His special research interests include integral equation methods for electromagnetic problems and periodic structure analysis.

**Zhengrui Li** received the B.S. degree in Communication and Information System from Beijing Jiaotong University, Beijing, China, in 1984; the M.S. degree in Electrical Engineering from the Communication University of China, Beijing, China, in 1987; and the Ph.D. degree in Electrical Engineering from Beijing Jiaotong University, Beijing, China, in 2009.

He is currently a Professor with the Communication University of China, Beijing, China. His research interests include the areas of computational electromagnetics, the Finite-Difference Time-Domain (FDTD) methods, electromagnetic modeling and simulation of antennas, and communication antennas. Li is a Senior Member of the Chinese Institute of Electronics.

**Yaoqing (Lamar) Yang** received his B.S. degree from the Beijing Jiaotong University, China, in 1983, and his M.S. degree from the Communication University of China, China, in 1986, both in Electrical Engineering. He received his Ph.D. degree in the area of Wireless Communications and Networks from the University of Texas (UT) at Austin in 2006.

He is now an Associate Professor in the Department of Computer and Electronics Engineering, University of Nebraska-Lincoln (UNL). His current research interests lie in wireless communications and networks with emphasis on radio channel characterizations, cognitive radio networks, and statistical signal processing. Yang is a Senior Member of IEEE.

**Guizhen Lu** was born in Beijing, China in 1957. He graduated from Peking University, Beijing, China, in 1984. From 1985 to present, he was with the Communication University of China. Now, he is a Professor in the same university. His main research interests are EMC and microwave technology.